Astron. Astrophys. 148, 123–132 (1985)

ASTRONOMY AND ASTROPHYSICS

Models of solar magnetic fluxtubes: constraints imposed by Fe I and II lines

S. K. Solanki and J. O. Stenflo*

Institute of Astronomy, ETH Zentrum, CH-8092 Zürich, Switzerland

Received November 22, 1984; accepted January 26, 1985

Summary. The diagnostic contents of the Stokes *I* and *V* profiles of about 50 unblended Fe II lines have been explored and used to set new constraints on the temperature structure of magnetic fluxtubes. The simultaneous use of Fe I and II lines allows us to determine the temperature in both the upper and lower fluxtube photosphere. The Fe II lines further make it possible to obtain model-insensitive values of the magnetic filling factors.

Empirically determined effective Landé factors of most of the unblended iron lines in the visible part of the solar spectrum are presented and compared with the corresponding LS coupling values.

Key words: solar magnetic fields – fluxtubes – Fe I and II – active regions – network – Landé factors

1. Introduction

In a previous paper (Solanki and Stenflo, 1984, to be referred to as Paper I) we presented a new approach to gaining insight into the structure of magnetic fluxtubes based on a statistical analysis of a large number of Stokes *I* and *V* profiles of lines belonging to the same element. This method, when applied to about 400 Fe I lines in Stokes *I* and *V* spectra obtained simultaneously with the Kitt Peak Fourier transform spectrometer used as a polarimeter, allowed us to partially separate the effects of magnetic field strength, magnetic filling factor, velocity fields, turbulence, and the temperature structure of the fluxtube. Thus, from preliminary calculations, using a very simple fluxtube model, we were able to make some estimates of the above quantities. In particular a difference in the temperature structure of plage and network fluxtubes was found, the plage fluxtubes being cooler in the deeper layers of the photosphere than their counterparts in the network.

The work presented in the present paper is a natural extension of Paper I, since Fe II lines respond differently from Fe I lines to the same physical conditions. Also, Fe I lines have some disadvantages. Their temperature sensitivity, which admits the distinction between plage and network temperatures in the lower layers of the atmosphere, does not allow a determination of the fluxtube temperature in the higher layers (see Paper I for details). This quantity can however be determined by considering Fe I and Fe II lines together. Since the Fe II lines are considerably less sensitive to temperature enhancements, they reduce the model dependence of the values of the magnetic filling factor derived through comparison of the Stokes *V* and *I* data.

2. Observations and data reduction

2.1. Observations

We have used data obtained on April 29 and 30, 1979 with the Kitt Peak McMath telescope and the 1 m Fourier transform spectrometer (FTS), adapted to simultaneously record both intensity and polarization spectra (Stokes *I* and *V*). These data consist of five spectra of different features near disk center, each covering a wavelength range of about 1000 Å with high spectral resolution (between 360,000 and 500,000), a spatial resolution of 10″, and an integration time of between 30 min and 1 h. More details can be found in Stenflo et al. (1984).

2.2. Summary of the reduction procedure

The reduction procedure used in the present work closely follows the one outlined in Paper I. We shall therefore only summarize it briefly, referring the interested reader to Paper I for further details.

The basis for the analysis of the Stokes *V* data is a first order relation between the intensity and polarization line profiles produced in a magnetic element, I_V and V respectively. The index V in I_V stresses the fact that this intensity profile refers to the same spatial region as Stokes *V*, and thus is not the same as Stokes *I*. In its integrated form, this relation reads

$$\frac{I_c - I_V}{I_c} = -\frac{1}{\Delta\lambda_H}\int_{\lambda_1}^{\lambda}\frac{V(\lambda')}{I_c}d\lambda', \quad (1)$$

where I_c is the intensity of the continuum, λ the wavelength, λ_1 the lower integration boundary, chosen to lie sufficiently far in the blue wing for V to approach zero, and $\Delta\lambda_H$ is the Zeeman splitting given by

$$\Delta\lambda_H = 4.67\,10^{-13}\,g\lambda^2 B \quad (2)$$

with λ and $\Delta\lambda_H$ in Å, and B in G. For lines with anomalous Zeeman splitting g must be replaced by the effective Landé factor g_{eff}. (1) is valid for weak magnetic fields, i.e. when the Zeeman splitting of a line is small compared with its width. This weak field approximation is valid for most lines, even in the presence of kilogauss fields (Stenflo et al., 1984).

Send offprint requests to: J. O. Stenflo

* Visiting astronomer, National Solar Observatory operated by Association of Universities for Research in Astronomy, Inc., under contract with the National Science Foundation

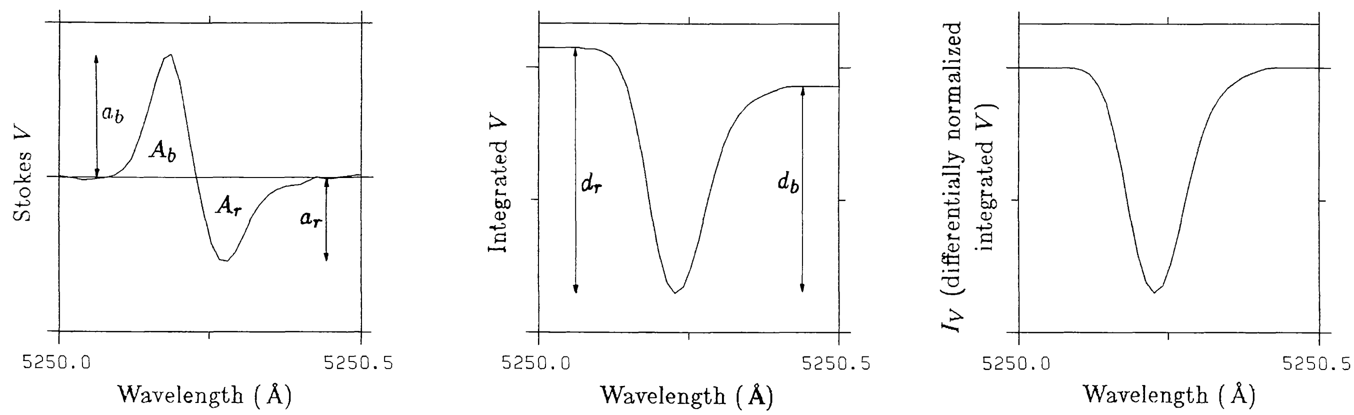

Fig. 1. Illustration of the transformation of a Stokes V profile into an I_V profile (Stokes I of the light from the fluxtube) using Eq. (1) for the Fe I 5250.2 Å line measured in a network element. Left: Asymmetric V profile of a spectral line. A_b and A_r are the areas of the blue and red wings of V, respectively, while a_b and a_r are their amplitudes. Center: Integrated V profile (before differential renormalization). d_b and d_r are the line depths measured from the blue and the red continuum, respectively. Right: I_V profile, i.e., integrated V after differential renormalization such that the continuum appears at a single level (see text)

If the fluxtubes are not spatially resolved, as is the case in our data, we have to replace I_V by $\langle I_V \rangle$ and B by $\langle B \rangle$ in $\Delta\lambda_H$, where $\langle B \rangle$ is the field strength averaged over the whole resolution element ($\langle B \rangle$ is proportional to the magnetic flux), and $\langle I_V \rangle$ is the intensity profile averaged over the *magnetic* elements inside the observed area. In a simple two component model of a magnetic region, composed of a magnetic component with no horizontal variations and with field strength B covering a fraction α (the magnetic filling factor) of the surface, and field free regions covering a fraction $(1-\alpha)$, we have: $\langle B \rangle = \alpha B$ and $\langle I_V \rangle = I_V$. In a more realistic model the magnetic field strength and the spectral intensity will vary smoothly across the diameters of the fluxtubes. Then

$$\langle B \rangle = \frac{\int B(x,y)\,dxdy}{\int dxdy}, \tag{3}$$

$$\langle I_V \rangle = \frac{\int B(x,y) I(x,y) dxdy}{\int B(x,y) dxdy}, \tag{4}$$

where x and y are coordinates in the plane perpendicular to the line of sight. Notice that I can occur without index V under the integral sign in (4). The weighting is such that only the magnetic areas contribute to $\langle I_V \rangle$. Of course (4) is only valid in the weak field approximation, since for strong fields V and I_V do not scale linearly with B. In the following we will use the symbols B, $\langle B \rangle$, $\langle I_V \rangle$, and I_V as representing the simple two component model.

A glance at (1) and (2) shows that a knowledge of the value of $\langle B \rangle$ is required if absolute values of I_V are to be determined. The Fe I lines of Paper I are too dependent on the temperature to be reliably used to determine $\langle B \rangle$. Although Fe II lines are much better in this respect, any uncalibrated depolarization in the instrument may still falsify the values of $\langle B \rangle$ determined from Stokes V. For this reason and for the sake of consistency with Paper I, we have opted for the use of the arbitrary scale factor of $\langle B \rangle = 1$ G in this investigation as well. As was already pointed out in Paper I this does not affect the analysis of the line profiles as long as the results are derived exclusively from a comparison of the relative profiles with each other.

As in Paper I the asymmetries of the Stokes V profiles (difference between the areas, A_r and A_b, and amplitudes, a_r and a_b, of the red and blue wings of Stokes V) lead us to renormalize the continuum of I_V by multiplying the blue wing of V by $\sqrt{A_r/A_b}$ and the red wing of V by $\sqrt{A_b/A_r}$ before integration. This renormalization forces the continuum on both sides of the I_V profile to lie at the same height, allowing the line to be uniquely parameterized in the same way as the I profile. Figure 1 illustrates this process for the Fe I 5250.2 Å line measured in a network element.

The renormalization process may affect the profiles in subtle ways. For example we only compensate for the area asymmetry of Stokes V, so that the amplitude asymmetry (which is not linearly related to the area asymmetry, cf. Fig. 12 of Paper I) could change the shape of the profile. Therefore, in order to get a feeling for the way in which this renormalization process affects the results, we have made test runs using unrenormalized I_V profiles as the basis of our statistical analysis. The parameterization is then no longer unique with, for example, two different line depth values possible per line (see Fig. 1). Using either of these values does not change the determined temperature structure by more than a few percent. Also, the values of the magnetic field strength and the magnetic filling factor are not affected strongly.

2.3. *The chosen lines and their Landé factors*

The set of Fe II lines used here has been taken from Dravins and Larsson (1984), who list 58 unblended Fe II lines in the wavelength range between 4120 and 6520 Å. Four of these lines could not be used in this investigation due to missing atomic data. The remaining lines are listed in Table 1. Column 1 contains the solar wavelength in Å, column 2 the multiplet number, column 3 the transition, column 4 the effective Landé factor ($g_{\rm eff}$) in LS coupling obtained from the tables of Beckers (1969c), and column 5 the $g_{\rm eff}$ values determined from the empirical Landé factors of the upper and lower levels of the transition. The expression for $g_{\rm eff}$ is

$$g_{\rm eff} = \tfrac{1}{2}(g_l + g_u) + \tfrac{1}{4}(g_l - g_u)\,(J_l(J_l+1) - J_u(J_u+1)), \tag{5}$$

where g_l and g_u are the Landé factors of the lower and upper levels of the transition, and J_l and J_u are the corresponding total angular momentum quantum numbers. According to Landi Degl'Innocenti (1982), (5) is also valid for cases where LS coupling does not apply, if the correct values for g_l and g_u are used [for example g_l and g_u values determined by laboratory measurements, as listed by Reader and Sugar (1975)].

For most of the listed lines the LS coupling and empirical Landé factors have similar values. Differences of 30% or more in

Table 1. List of Fe II lines and their Landé factors

Wavelength	Multiplet	Transition	$g_{eff\,LS}$	$g_{eff\,emp}$	Wavelength	Multiplet	Transition	$g_{eff\,LS}$	$g_{eff\,emp}$
4122.6625	28	$b\,^4P_{2\frac{1}{2}} - z\,^4F^{\circ}_{2\frac{1}{2}}$	1.314	1.326	5100.6563	35	$b\,^4F_{4\frac{1}{2}} - z\,^6F^{\circ}_{3\frac{1}{2}}$	1.222	1.146
4124.7842	22	$a\,^2D_{2\frac{1}{2}} - z\,^4F^{\circ}_{3\frac{1}{2}}$	1.286	1.377	5132.6658	35	$b\,^4F_{4\frac{1}{2}} - z\,^6F^{\circ}_{4\frac{1}{2}}$	1.384	1.368
4128.7410	27	$b\,^4P_{2\frac{1}{2}} - z\,^4D^{\circ}_{1\frac{1}{2}}$	1.900	1.908	5136.7971	35	$b\,^4F_{2\frac{1}{2}} - z\,^6F^{\circ}_{1\frac{1}{2}}$	1.000	1.003
4178.8590	28	$b\,^4P_{2\frac{1}{2}} - z\,^4F^{\circ}_{3\frac{1}{2}}$	0.786	0.924	5197.5742	49	$a\,^4G_{2\frac{1}{2}} - z\,^4F^{\circ}_{1\frac{1}{2}}$	0.700	0.671
4258.1590	28	$b\,^4P_{1\frac{1}{2}} - z\,^4F^{\circ}_{1\frac{1}{2}}$	1.067	1.082	5234.6298	49	$a\,^4G_{3\frac{1}{2}} - z\,^4F^{\circ}_{2\frac{1}{2}}$	0.929	0.869
4369.4030	28	$b\,^4P_{\frac{1}{2}} - z\,^4F^{\circ}_{1\frac{1}{2}}$	−0.167	−0.114	5256.9346	41	$a\,^6S_{2\frac{1}{2}} - z\,^6F^{\circ}_{2\frac{1}{2}}$	1.657	1.650
4413.5941	32	$a\,^4H_{4\frac{1}{2}} - z\,^4F^{\circ}_{4\frac{1}{2}}$	1.152	1.135	5264.8074	48	$a\,^4G_{2\frac{1}{2}} - z\,^4D^{\circ}_{1\frac{1}{2}}$	0.100	0.142
4416.8245	27	$b\,^4P_{\frac{1}{2}} - z\,^4D^{\circ}_{1\frac{1}{2}}$	0.833	0.767	5284.1091	41	$a\,^6S_{2\frac{1}{2}} - z\,^4F^{\circ}_{3\frac{1}{2}}$	1.071	0.653
4491.4035	37	$b\,^4F_{1\frac{1}{2}} - z\,^4F^{\circ}_{1\frac{1}{2}}$	0.400	0.421	5325.5558	49	$a\,^4G_{3\frac{1}{2}} - z\,^4F^{\circ}_{3\frac{1}{2}}$	1.111	1.135
4508.2866	38	$b\,^4F_{1\frac{1}{2}} - z\,^4D^{\circ}_{\frac{1}{2}}$	0.500	0.503	5337.7364	48	$a\,^4G_{2\frac{1}{2}} - z\,^4D^{\circ}_{2\frac{1}{2}}$	0.971	0.962
4515.3389	37	$b\,^4F_{2\frac{1}{2}} - z\,^4F^{\circ}_{2\frac{1}{2}}$	1.029	1.044	5414.0736	48	$a\,^4G_{3\frac{1}{2}} - z\,^4D^{\circ}_{3\frac{1}{2}}$	1.206	1.190
4520.2258	37	$b\,^4F_{4\frac{1}{2}} - z\,^4F^{\circ}_{3\frac{1}{2}}$	1.500	1.336	5425.2523	49	$a\,^4G_{4\frac{1}{2}} - z\,^4F^{\circ}_{4\frac{1}{2}}$	1.253	1.235
4534.1639	37	$b\,^4F_{1\frac{1}{2}} - z\,^4F^{\circ}_{2\frac{1}{2}}$	1.500	1.572	5534.8451	55	$b\,^2H_{5\frac{1}{2}} - z\,^4F^{\circ}_{4\frac{1}{2}}$	0.545	0.572
4541.5204	38	$b\,^4F_{1\frac{1}{2}} - z\,^4D^{\circ}_{1\frac{1}{2}}$	0.800	0.774	5824.4065	58	$a\,^2F_{2\frac{1}{2}} - z\,^4D^{\circ}_{2\frac{1}{2}}$	1.114	1.100
4555.8937	37	$b\,^4F_{3\frac{1}{2}} - z\,^4F^{\circ}_{3\frac{1}{2}}$	1.238	1.250	5991.3749	46	$a\,^4G_{5\frac{1}{2}} - z\,^6F^{\circ}_{4\frac{1}{2}}$	0.909	0.803
4576.3377	38	$b\,^4F_{2\frac{1}{2}} - z\,^4D^{\circ}_{2\frac{1}{2}}$	1.200	1.184	6084.1061	46	$a\,^4G_{4\frac{1}{2}} - z\,^6F^{\circ}_{3\frac{1}{2}}$	0.778	0.714
4582.8330	37	$b\,^4F_{2\frac{1}{2}} - z\,^4F^{\circ}_{3\frac{1}{2}}$	1.500	1.629	6113.3221	46	$a\,^4G_{3\frac{1}{2}} - z\,^6F^{\circ}_{2\frac{1}{2}}$	0.571	0.575
4620.5160	38	$b\,^4F_{3\frac{1}{2}} - z\,^4D^{\circ}_{3\frac{1}{2}}$	1.333	1.305	6149.2483	74	$b\,^4D_{\frac{1}{2}} - z\,^4P^{\circ}_{\frac{1}{2}}$	1.333	—
4635.3100	186	$d\,^2D_{2\frac{1}{2}} - y\,^2F^{\circ}_{3\frac{1}{2}}$	1.071	—	6238.3903	74	$b\,^4D_{1\frac{1}{2}} - z\,^4P^{\circ}_{1\frac{1}{2}}$	1.467	—
4656.9787	43	$a\,^6S_{2\frac{1}{2}} - z\,^4D^{\circ}_{2\frac{1}{2}}$	1.686	1.673	6239.9431	74	$b\,^4D_{\frac{1}{2}} - z\,^4P^{\circ}_{1\frac{1}{2}}$	2.167	—
4666.7536	37	$b\,^4F_{3\frac{1}{2}} - z\,^4F^{\circ}_{4\frac{1}{2}}$	1.500	1.512	6247.5643	74	$b\,^4D_{2\frac{1}{2}} - z\,^4P^{\circ}_{1\frac{1}{2}}$	1.100	1.034
4670.1723	25	$b\,^4P_{2\frac{1}{2}} - z\,^6F^{\circ}_{3\frac{1}{2}}$	1.143	1.169	6369.4619	40	$a\,^6S_{2\frac{1}{2}} - z\,^6D^{\circ}_{1\frac{1}{2}}$	2.100	2.098
4720.1347	54	$b\,^2P_{1\frac{1}{2}} - z\,^4P^{\circ}_{2\frac{1}{2}}$	1.800	1.788	6416.9282	74	$b\,^4D_{2\frac{1}{2}} - z\,^4P^{\circ}_{2\frac{1}{2}}$	1.486	1.459
4833.1919	30	$a\,^4H_{5\frac{1}{2}} - z\,^6F^{\circ}_{4\frac{1}{2}}$	0.455	0.419	6432.6831	40	$a\,^6S_{2\frac{1}{2}} - z\,^6D^{\circ}_{2\frac{1}{2}}$	1.829	1.824
4893.8136	36	$b\,^4F_{3\frac{1}{2}} - z\,^6P^{\circ}_{2\frac{1}{2}}$	0.429	0.386	6446.4102	199	$c\,^4F_{3\frac{1}{2}} - x\,^4G^{\circ}_{4\frac{1}{2}}$	1.056	—
4923.9299	42	$a\,^6S_{2\frac{1}{2}} - z\,^6P^{\circ}_{1\frac{1}{2}}$	1.700	1.694	6456.3878	74	$b\,^4D_{3\frac{1}{2}} - z\,^4P^{\circ}_{2\frac{1}{2}}$	1.214	1.182
4993.3527	36	$b\,^4F_{4\frac{1}{2}} - z\,^6P^{\circ}_{3\frac{1}{2}}$	0.667	0.616	6516.0855	40	$a\,^6S_{2\frac{1}{2}} - z\,^6D^{\circ}_{3\frac{1}{2}}$	1.071	1.069

g_{eff} are only present for the lines at 4369.4, 5264.8, and 5284.1 Å. These lines can be used to check the empirical method of determining g_{eff} using the $\ln(d_V/d_I)$ vs. S_I plot, as outlined in Sect. 2.3 of Paper I (d_I and S_I are the line depth and line strength of the I profile, and d_V is the line depth of the I_V profile). If the LS coupling g_{eff} value of the 5284.1 Å line is used in $\Delta\lambda_H$, then d_V turns out to be much too small in a plot of $\ln(d_V/d_I)$ vs. S_I. By using the g_{eff} value listed in column 5 a larger line depth of I_V is obtained, and then the corresponding point fits in with the remaining points in the $\ln(d_V/d_I)$ vs. S_I scatter plot. The two other lines unfortunately cannot be used in the same way as a check, since their g_{eff} values are very small. This makes their V profiles very weak and thus easily affected by noise in the data.

Noise is a serious problem for some other lines with weak V profiles too, so they have been removed. Finally the lines 4534.16 and 4258.16 Å have been omitted from the analysis as well, since their V profiles are seriously affected by blends in the wings.

Since part of our analysis (filling factors, cf. Sect. 4 and Paper I) is very sensitive to the value of the Landé factors, we have determined the effective Landé factors of all those unblended Fe I lines of Stenflo and Lindegren (1977), for which the empirical g_l and g_u values are available from laboratory measurements (Corliss and Sugar, 1982; Reader and Sugar, 1975; Moore, 1952; Litzén, 1984). The results are presented in Table 2, which is structured as Table 1. A question mark has been placed behind the g_{eff} values in the last column of those lines for which the empirical Landé factors of one of their levels have been measured with lower accuracy than usual. The difference between the LS coupling and empirical g_{eff} values is again mostly negligible. However, for the following lines the relative difference is greater than 30%: 4560.1, 4596.4, 4798.3, 4954.6, 5236.2, 5560.2, 5624.0, 5677.7, 5686.5, 5717.8, 6008.0, and 6165.4 Å. Ten of these lines have not been discussed in Paper I. There are two main reasons why their g_{eff} values were not recognized to be wrong then: (1) Most of them have small g_{eff} values. This combined with the fact that some of them have relatively small line strengths as well means that their V profiles are weak and easily affected by noise. Therefore we hesitated to attribute deviations to departures from LS coupling. (2) The relative differences between the LS coupling g_{eff} values of these lines are on the whole considerably smaller than those of the lines discussed in Paper I. Therefore the $\ln(d_V/d_I)$ values of these lines lie much closer to those of normal lines and consequently their abnormality is harder to detect.

However, now that we know that these 10 lines are prime candidates for departures from LS coupling, we can use them to test the validity of the empirical Landé factors derived in Paper I with the statistical technique. We find that except for two of them the g_{eff} values determined from laboratory measurements and

Table 2. List of Fe I lines and their Landé factors

Wavelength	Multiplet	Transition	$g_{eff\,LS}$	$g_{eff\,emp}$
4365.9004	415	$b\,^3G_4 - w\,^3D_3^o$	0.625	0.601
4389.2512	2	$a\,^5D_3 - z\,^7F_2^o$	1.500	1.497
4432.5726	797	$a\,^1H_5 - u\,^3G_5^o$	1.100	1.070
4439.6371	515	$a\,^1G_4 - x\,^3F_3^o$	0.875	0.884
4439.8860	116	$a\,^3P_2 - z\,^5S_2^o$	1.750	1.745
4442.8357	69	$a\,^5P_3 - y\,^7P_2^o$	1.000	0.992
4443.1998	350	$b\,^3P_0 - x\,^3D_1^o$	0.500	0.556
4445.4760	2	$a\,^5D_2 - z\,^7F_2^o$	1.500	1.502
4447.1354	69	$a\,^5P_2 - y\,^7P_3^o$	2.000	1.996
4484.2266	828	$z\,^5P_3^o - g\,^5D_4$	1.250	1.232
4489.7449	2	$a\,^5D_0 - z\,^7F_1^o$	1.500	1.549
4502.5931	796	$a\,^1H_5 - x\,^3H_6^o$	1.583	1.563
4523.4015	829	$z\,^5P_2^o - e\,^7S_3$	2.167	2.00?
4537.6723	594	$b\,^3H_5 - z\,^1H_5^o$	1.017	1.025
4556.9275	638	$a\,^3D_3 - v\,^5P_2^o$	0.833	0.930
4560.0909	823	$z\,^5P_3^o - e\,^5G_4$	0.375	0.609
4574.2191	554	$z\,^5D_4^o - e\,^5F_3$	1.875	1.901
4574.7224	115	$a\,^3P_2 - x\,^5D_2^o$	1.500	1.503
4587.1316	795	$a\,^1H_5 - x\,^1G_4^o$	1.000	1.044
4596.4113	823	$z\,^5P_2^o - e\,^5G_3$	0.000	0.753
4598.1221	554	$z\,^5D_1^o - e\,^5F_1$	0.750	0.751
4602.0060	39	$a\,^3F_2 - y\,^5F_1^o$	1.000	1.013
4602.9466	39	$a\,^3F_4 - y\,^5F_5^o$	1.700	1.743
4619.2932	821	$z\,^5P_3^o - f\,^5D_2$	1.833	1.700
4625.0514	554	$z\,^5D_3^o - e\,^5F_3$	1.375	1.368
4630.1258	115	$a\,^3P_2 - x\,^5D_3^o$	1.500	1.502
4635.8509	349	$b\,^3P_1 - y\,^5S_2^o$	2.250	2.087
4637.5095	554	$z\,^5D_1^o - e\,^5F_2$	0.750	0.739
4657.5879	346	$b\,^3P_1 - w\,^5D_1^o$	1.500	1.402
4658.2976	591	$b\,^3H_5 - x\,^3G_4^o$	1.000	0.974
4672.8364	40	$a\,^3F_2 - z\,^3P_1^o$	0.250	0.257
4678.8519	821	$z\,^5P_3^o - f\,^5D_4$	1.250	1.299
4683.5638	346	$b\,^3P_2 - w\,^5D_2^o$	1.500	1.515
4700.1590	935	$b\,^1G_4 - x\,^3H_5^o$	1.100	1.156
4704.9519	821	$z\,^5P_1^o - f\,^5D_0$	2.500	2.487
4726.1396	384	$z\,^7P_3^o - e\,^5D_2$	2.333	2.313
4733.5968	38	$a\,^3F_4 - y\,^5D_4^o$	1.375	1.375
4735.8471	1042	$c\,^3F_4 - t\,^3G_5^o$	1.100	1.174
4741.5341	346	$b\,^3P_2 - w\,^5D_3^o$	1.500	1.464
4749.9488	1206	$y\,^5P_3^o - i\,^5D_3$	1.583	1.538
4776.0702	635	$a\,^3D_2 - y\,^3S_1^o$	0.750	0.825
4779.4423	720	$a\,^1P_1 - x\,^3P_0^o$	1.000	0.817
4780.8132	633	$a\,^3D_3 - w\,^3D_2^o$	1.500	1.454
4786.8127	467	$c\,^3P_2 - x\,^3D_3^o$	1.167	1.220
4788.7627	588	$b\,^3H_6 - z\,^3H_6^o$	1.167	1.182
4789.6568	753	$a\,^1D_2 - z\,^1D_2^o$	1.000	0.97?
4790.7436	632	$a\,^3D_3 - x\,^3F_3^o$	1.208	1.247
4794.3571	115	$a\,^3P_1 - x\,^5D_1^o$	1.500	1.499
4798.2670	1042	$c\,^3F_2 - t\,^3G_3^o$	0.833	1.167
4798.7336	38	$a\,^3F_2 - y\,^5D_2^o$	1.083	1.082
4799.0698	1098	$y\,^5F_2^o - f\,^3F_2$	0.833	0.837
4807.7122	688	$z\,^5F_4^o - e\,^3F_4$	1.300	1.321
4808.1509	633	$a\,^3D_3 - w\,^3D_3^o$	1.333	1.340
4809.9400	793	$a\,^1H_5 - y\,^3H_5^o$	1.017	1.037
4839.5500	588	$b\,^3H_5 - z\,^3H_5^o$	1.033	1.046
4848.8866	114	$a\,^3P_2 - y\,^3D_1^o$	2.000	2.012
4871.3262	318	$z\,^7F_3^o - e\,^7D_2$	1.000	1.017
4873.7534	633	$a\,^3D_2 - w\,^3D_2^o$	1.167	1.197
4874.3565	467	$c\,^3P_1 - x\,^3D_2^o$	1.000	1.067
4875.8815	687	$z\,^5F_5^o - e\,^5F_4$	1.500	1.535
4882.1484	687	$z\,^5F_2^o - e\,^5F_2$	1.000	0.997
4885.4301	966	$z\,^3F_4^o - g\,^5D_3$	0.875	0.887
4907.7365	687	$z\,^5F_1^o - e\,^5F_2$	1.500	1.492
4909.3874	985	$z\,^3D_2^o - g\,^5D_2$	1.333	1.37?
4910.0222	687	$z\,^5F_3^o - e\,^5F_3$	1.250	1.243
4911.7808	984	$z\,^3D_2^o - e\,^3D_1$	1.500	1.351
4938.8209	318	$z\,^7F_2^o - e\,^7D_3$	2.000	2.006
4939.6931	16	$a\,^5F_5 - z\,^5F_4^o$	1.500	1.491
4945.6390	1113	$z\,^3P_2^o - f\,^5G_3$	0.333	0.791
4946.3941	687	$z\,^5F_4^o - e\,^5F_4$	1.350	1.343
4950.1108	687	$z\,^5F_2^o - e\,^5F_3$	1.500	1.468
4962.5756	1097	$y\,^5F_5^o - e\,^3H_6$	0.583	0.745
4985.2587	984	$z\,^3D_2^o - e\,^3D_2$	1.167	1.146
4985.5530	318	$z\,^7F_3^o - e\,^7D_4$	1.875	1.868
4994.1364	16	$a\,^5F_4 - z\,^5F_3^o$	1.500	1.500
4999.1135	1040	$c\,^3F_2 - x\,^1F_3^o$	1.333	1.481
5001.8760	965	$z\,^3F_4^o - e\,^3D_3$	1.125	1.107

Table 2 (continued)

Wavelength	Multiplet	Transition	$g_{eff\,LS}$	$g_{eff\,emp}$
5002.7985	687	$z\,^5F_3^o - e\,^5F_4$	1.500	1.452
5012.6983	1093	$y\,^5F_2^o - e\,^5H_3$	0.000	−0.030
5014.9505	965	$z\,^3F_3^o - e\,^3D_2$	1.000	1.047
5022.2420	965	$z\,^3F_2^o - e\,^3D_1$	0.750	0.622
5029.6208	718	$a\,^1P_1 - \,^1D_2^o$	1.000	1.30?
5030.7807	585	$b\,^3H_6 - z\,^3I_7^o$	1.071	1.101
5044.2164	318	$z\,^7F_4^o - e\,^7D_5$	1.800	1.769
5048.4413	984	$z\,^3D_1^o - e\,^3D_2$	1.500	1.431
5058.4987	884	$b\,^3D_3 - v\,^3D_3^o$	1.333	1.268
5072.6767	1095	$y\,^5F_4^o - f\,^3D_3$	1.375	1.473
5074.7556	1094	$y\,^5F_4^o - e\,^3G_5$	0.900	1.056
5079.7462	16	$a\,^5F_2 - z\,^5F_1^o$	1.500	1.505
5083.3450	16	$a\,^5F_3 - z\,^5F_3^o$	1.250	1.250
5088.1559	1066	$y\,^5D_3^o - h\,^5D_4$	1.500	1.349
5104.0338	465	$c\,^3P_2 - w\,^5D_3^o$	1.500	1.478
5104.1916	1092	$y\,^5F_5^o - f\,^5G_5$	1.333	1.319
5127.3655	16	$a\,^5F_4 - z\,^5F_5^o$	1.500	1.497
5127.6836	1	$a\,^5D_3 - z\,^7D_2^o$	1.000	0.993
5129.6312	965	$z\,^3F_3^o - e\,^3D_3$	1.208	1.215
5136.0929	1036	$c\,^3F_2 - z\,^1P_1^o$	0.500	0.382
5137.3897	1090	$y\,^5F_5^o - h\,^5D_4$	1.200	1.381
5141.7460	114	$a\,^3P_1 - y\,^3D_1^o$	1.000	0.996
5143.7250	65	$a\,^5P_2 - y\,^3F_3^o$	0.333	0.352
5145.0993	66	$a\,^5P_2 - y\,^5P_2^o$	1.833	1.828
5194.9477	36	$a\,^3F_3 - z\,^3F_3^o$	1.083	1.086
5198.7171	66	$a\,^5P_1 - y\,^5P_2^o$	1.500	1.504
5213.8071	962	$z\,^3F_3^o - e\,^5G_4$	1.250	1.466
5216.2802	36	$a\,^3F_2 - z\,^3F_2^o$	0.667	0.676
5217.3972	553	$z\,^5D_4^o - e\,^5D_3$	1.500	1.493
5225.5332	1	$a\,^5D_1 - z\,^7D_1^o$	2.250	2.250
5232.9493	383	$z\,^7P_4^o - e\,^7D_5$	1.300	1.261
5236.2039	1034	$c\,^3F_2 - \,^3P_1^o$	0.250	0.39?
5242.4988	843	$a\,^1I_6 - z\,^1H_5^o$	1.000	1.004
5247.0585	1	$a\,^5D_2 - z\,^7D_3^o$	2.000	1.992
5250.2171	1	$a\,^5D_0 - z\,^7D_1^o$	3.000	2.999
5250.6527	66	$a\,^5P_2 - y\,^5P_3^o$	1.500	1.502
5253.0250	113	$a\,^3P_2 - y\,^5P_1^o$	1.000	1.008
5253.4693	553	$z\,^5D_1^o - e\,^5D_1$	1.500	1.506
5262.6240	1149	$z\,^5G_6^o - e\,^3H_6$	1.250	1.278
5263.3143	553	$z\,^5D_2^o - e\,^5D_2$	1.500	1.503
5279.6578	584	$b\,^3H_4 - y\,^3G_3^o$	0.875	0.880
5284.6100	1032	$c\,^3F_2 - t\,^3D_2^o$	0.917	0.911
5288.5315	929	$b\,^1G_4 - y\,^1G_4^o$	1.000	1.021
5293.9609	1031	$c\,^3F_3 - u\,^3D_2^o$	1.000	0.976
5295.3160	1146	$z\,^5G_3^o - e\,^5H_3$	0.708	0.685
5302.3074	553	$z\,^5D_1^o - e\,^5D_2$	1.500	1.507
5320.0381	877	$b\,^3D_3 - v\,^5P_2^o$	0.833	0.912
5321.1105	1165	$z\,^3G_4^o - e\,^3H_4$	0.925	0.985
5322.0461	112	$a\,^3P_2 - y\,^3F_3^o$	0.667	0.666
5329.9932	1028	$c\,^3F_4 - \,^1H_5^o$	0.500	0.65?
5332.9062	36	$a\,^3F_3 - z\,^3F_4^o$	1.500	1.496
5339.9356	553	$z\,^5D_2^o - e\,^5D_3$	1.500	1.513
5358.1168	628	$a\,^3D_2 - x\,^3D_2^o$	1.167	1.189
5364.8801	1146	$z\,^5G_2^o - e\,^5H_3$	0.667	0.633
5365.4063	786	$a\,^1H_5 - z\,^1G_4^o$	1.000	0.950
5367.4755	1146	$z\,^5G_3^o - e\,^5H_4$	0.875	0.92?
5369.9702	1146	$z\,^5G_4^o - e\,^5H_5$	1.000	1.100
5373.7136	1166	$z\,^3G_3^o - f\,^3F_4$	2.000	1.666
5379.5796	928	$b\,^1G_4 - z\,^1H_5^o$	1.000	1.096
5383.3792	1146	$z\,^5G_5^o - e\,^5H_6$	1.083	1.123
5389.4866	1145	$z\,^5G_3^o - f\,^5G_3$	0.917	1.014
5393.1744	553	$z\,^5D_3^o - e\,^5D_4$	1.500	1.517
5405.7838	15	$a\,^5F_2 - z\,^5D_1^o$	0.750	0.752
5406.7799	1148	$z\,^5G_4^o - f\,^3D_3$	0.875	0.870
5410.9197	1165	$z\,^3G_3^o - e\,^3H_4$	0.875	0.991
5412.7876	1162	$z\,^3G_4^o - e\,^5H_4$	0.975	1.00?
5415.2108	1165	$z\,^3G_5^o - e\,^3H_6$	1.083	1.167
5422.1560	1145	$z\,^5G_6^o - f\,^5G_5$	1.500	1.609
5434.5315	15	$a\,^5F_1 - z\,^5D_0^o$	0.000	−0.014
5436.5926	113	$a\,^3P_2 - y\,^5P_3^o$	1.833	1.816
5441.3420	1144	$z\,^5G_5^o - h\,^5D_4$	0.800	0.784
5445.0502	1163	$z\,^3G_5^o - e\,^3G_5$	1.200	1.248
5460.8762	464	$c\,^3P_1 - x\,^5P_1^o$	2.000	1.965
5461.5530	1145	$z\,^5G_2^o - f\,^5G_3$	1.500	1.949
5462.9672	1163	$z\,^3G_3^o - e\,^3G_3$	0.750	0.816
5463.2851	1163	$z\,^3G_4^o - e\,^3G_4$	1.050	1.098
5464.2825	1030	$c\,^3F_3 - y\,^1D_2^o$	1.167	1.107

Table 2 (continued)

Wavelength	Multiplet	Transition	$g_{eff_{LS}}$	$g_{eff_{emp}}$
5473.9076	1062	$y\,^5D^o_3 - g\,^5D_3$	1.500	1.492
5483.1017	1061	$y\,^5D^o_3 - e\,^3D_2$	1.833	1.859
5491.8346	1031	$c\,^3F_2 - u\,^3D^o_3$	2.000	1.935
5493.5012	1061	$y\,^5D^o_4 - e\,^3D_3$	1.750	1.722
5494.4668	1024	$c\,^3F_4 - x\,^3H^o_5$	0.600	0.586
5501.4715	15	$a\,^5F_3 - z\,^5D^o_4$	1.875	1.880
5506.7864	15	$a\,^5F_2 - z\,^5D^o_3$	2.000	2.000
5522.4491	1108	$z\,^3P^o_2 - g\,^5D_2$	1.500	1.53?
5543.1944	926	$b\,^1G_4 - x\,^3G^o_5$	1.375	1.651
5543.9399	1062	$y\,^5D^o_1 - g\,^5D_2$	1.500	1.61?
5546.5101	1145	$z\,^5G^o_4 - f\,^5G_5$	1.500	1.457
5560.2156	1164	$z\,^3G^o_4 - f\,^3D_3$	0.625	0.863
5565.7114	1183	$y\,^3F^o_3 - f\,^3F_3$	1.083	1.078
5569.6253	686	$z\,^5F^o_2 - e\,^5D_1$	0.750	0.747
5576.0970	686	$z\,^5F^o_1 - e\,^5D_0$	0.000	−0.012
5587.5755	1026	$c\,^3F_3 - v\,^3F^o_4$	1.500	1.206
5607.6668	1058	$y\,^5D^o_3 - e\,^7G_4$	1.000	1.107
5618.6360	1107	$z\,^3P^o_2 - e\,^3D_2$	1.333	1.309
5619.6002	1161	$z\,^3G^o_5 - f\,^5G_6$	1.667	1.510
5624.0264	1160	$z\,^3G^o_5 - h\,^5D_4$	0.600	0.874
5633.9504	1314	$x\,^5F^o_5 - g\,^5G_6$	1.167	1.42?
5638.2675	1087	$y\,^5F^o_4 - g\,^5D_3$	1.125	1.122
5649.9878	1314	$x\,^5F^o_1 - g\,^5G_2$	0.500	0.517
5652.3194	1108	$z\,^3P^o_1 - g\,^5D_2$	1.500	1.61?
5662.5233	1087	$y\,^5F^o_5 - g\,^5D_4$	1.200	1.277
5677.6875	1057	$y\,^5D^o_4 - e\,^5G_5$	0.800	1.088
5679.0295	1183	$y\,^3F^o_2 - f\,^3F_3$	1.500	1.454
5680.2441	1026	$c\,^3F_2 - v\,^3F^o_3$	1.500	1.515
5686.5372	1182	$y\,^3F^o_4 - e\,^3H_5$	0.600	0.835
5701.5527	209	$b\,^3F_4 - y\,^3D^o_3$	1.125	1.101
5712.1361	686	$z\,^5F^o_2 - e\,^5D_3$	2.000	2.012
5717.8379	1107	$z\,^3P^o_0 - e\,^3D_1$	0.500	0.801
5720.8950	1178	$y\,^3F^o_4 - f\,^5G_3$	1.750	1.402
5724.4660	1109	$z\,^3P^o_0 - e\,^5P_1$	2.500	2.432
5731.7666	1087	$y\,^5F^o_3 - g\,^5D_3$	1.375	1.368
5741.8560	1086	$y\,^5F^o_3 - e\,^3D_2$	1.333	1.363
5752.0377	1180	$y\,^3F^o_4 - e\,^3G_4$	1.150	1.171
5753.1287	1107	$z\,^3P^o_1 - e\,^3D_2$	1.000	0.939
5759.2637	1184	$y\,^3F^o_2 - e\,^3P_2$	1.083	1.073
5760.3455	867	$b\,^3D_3 - y\,^3P^o_2$	1.167	1.208
5775.0849	1087	$y\,^5F^o_4 - g\,^5D_4$	1.425	1.415
5778.4579	209	$b\,^3F_3 - y\,^3D^o_3$	1.208	1.198
5780.6041	552	$z\,^5D^o_3 - e\,^7D_3$	1.625	1.627
5784.6614	686	$z\,^5F^o_3 - e\,^5D_4$	1.875	1.880
5793.9178	1086	$y\,^5F^o_4 - e\,^3D_3$	1.375	1.342
5804.0370	959	$z\,^3F^o_4 - e\,^3F_3$	1.500	1.464
5807.7868	552	$z\,^5D^o_0 - e\,^7D_1$	3.000	3.002
5809.2215	982	$z\,^3D^o_3 - e\,^3F_3$	1.208	1.214
5811.9172	1022	$c\,^3F_3 - x\,^1G^o_4$	0.875	0.846
5814.8092	1086	$y\,^5F^o_2 - e\,^3D_2$	1.083	1.061
5827.8794	552	$z\,^5D^o_1 - e\,^7D_2$	2.250	2.266
5835.1018	1084	$y\,^5F^o_3 - f\,^5F_4$	1.500	1.521?
5838.3753	959	$z\,^3F^o_3 - e\,^3F_2$	1.500	1.550
5849.6864	922	$b\,^1G_4 - x\,^3F^o_4$	1.125	1.161
5855.0803	1179	$y\,^3F^o_3 - e\,^5H_4$	0.625	0.62?
5858.7840	1084	$y\,^5F^o_4 - f\,^5F_5$	1.500	1.464
5859.5938	1181	$y\,^3F^o_4 - f\,^3D_3$	1.125	1.228
5862.3651	1180	$y\,^3F^o_4 - e\,^3G_5$	1.100	1.252
5881.2822	1178	$y\,^3F^o_3 - f\,^5G_3$	1.000	1.114
5916.2535	170	$a\,^3H_4 - y\,^3F^o_4$	1.025	1.028
5930.1894	1180	$y\,^3F^o_2 - e\,^3G_3$	0.833	0.996
5934.6619	982	$z\,^3D^o_2 - e\,^3F_3$	1.000	1.046
5952.7212	959	$z\,^3F^o_2 - e\,^3F_2$	0.667	0.652
5956.6997	14	$a\,^5F_5 - z\,^7P^o_4$	0.700	0.707
5976.7838	959	$z\,^3F^o_3 - e\,^3F_3$	1.083	1.096
5984.8221	1260	$y\,^3D^o_3 - e\,^3P_2$	1.167	1.189
5987.0674	1260	$y\,^3D^o_2 - e\,^3P_1$	1.000	0.997
6003.0188	959	$z\,^3F^o_4 - e\,^3F_4$	1.250	1.269
6007.9656	1178	$y\,^3F^o_2 - f\,^5G_3$	1.167	1.596
6008.5631	982	$z\,^3D^o_3 - e\,^3F_4$	1.125	1.238
6027.0562	1018	$c\,^3F_4 - v\,^3G^o_5$	1.100	0.961
6034.0365	1142	$z\,^5G^o_5 - g\,^5D_4$	0.800	0.680
6056.0114	1259	$y\,^3D^o_3 - f\,^3F_4$	1.125	0.866
6065.4921	207	$b\,^3F_2 - y\,^3F^o_2$	0.667	0.675
6078.4976	1259	$y\,^3D^o_2 - f\,^3F_3$	1.000	0.991
6082.7147	64	$a\,^5P_1 - z\,^3P^o_1$	2.000	1.997
6096.6682	959	$z\,^3F^o_2 - e\,^3F_3$	1.500	1.532
6102.1828	1259	$y\,^3D^o_1 - f\,^3F_2$	0.750	0.767
6136.6241	169	$a\,^3H_4 - z\,^3G^o_3$	0.875	0.841
6136.9992	62	$a\,^5P_2 - y\,^5D^o_1$	2.000	1.984
6137.7007	207	$b\,^3F_3 - y\,^3F^o_3$	1.083	1.079
6151.6217	62	$a\,^5P_3 - y\,^5D^o_2$	1.833	1.837
6157.7331	1015	$c\,^3F_4 - w\,^3F^o_4$	1.250	1.222
6165.3641	1018	$c\,^3F_3 - v\,^3G^o_4$	1.000	0.686
6173.3433	62	$a\,^5P_1 - y\,^5D^o_0$	2.500	2.499
6180.2084	269	$a\,^3G_4 - y\,^3D^o_3$	0.625	0.641
6187.9941	959	$z\,^3F^o_3 - e\,^3F_4$	1.500	1.591
6191.5680	169	$a\,^3H_5 - z\,^3G^o_4$	1.000	0.914
6200.3204	207	$b\,^3F_2 - y\,^3F^o_3$	1.500	1.509
6213.4375	62	$a\,^5P_1 - y\,^5D^o_1$	2.000	1.995
6219.2886	62	$a\,^5P_2 - y\,^5D^o_2$	1.667	1.657
6220.7867	958	$z\,^3F^o_4 - e\,^5F_4$	1.300	1.290
6226.7403	981	$z\,^3D^o_3 - e\,^5F_4$	1.375	1.346
6232.6493	816	$z\,^5P^o_2 - e\,^5D_1$	2.000	1.993
6240.6516	64	$a\,^5P_1 - z\,^3P^o_2$	1.000	0.990
6246.3271	816	$z\,^5P^o_3 - e\,^5D_3$	1.583	1.582
6252.5642	169	$a\,^3H_6 - z\,^3G^o_5$	1.083	0.950
6265.1412	62	$a\,^5P_3 - y\,^5D^o_3$	1.583	1.579
6270.2322	342	$b\,^3P_0 - y\,^3D^o_1$	0.500	0.493
6271.2832	685	$z\,^5F^o_5 - e\,^7D_5$	1.500	1.492
6280.6240	13	$a\,^5F_5 - z\,^7F^o_5$	1.450	1.449
6297.8013	62	$a\,^5P_1 - y\,^5D^o_2$	1.000	0.993
6301.5091	816	$z\,^5P^o_2 - e\,^5D_2$	1.667	1.669
6302.5017	816	$z\,^5P^o_1 - e\,^5D_0$	2.500	2.487
6303.4671	1140	$z\,^5G^o_6 - e\,^5G_5$	1.500	1.262
6311.5050	342	$b\,^3P_2 - y\,^3D^o_2$	1.333	1.324
6315.8164	1014	$c\,^3F_4 - y\,^1G^o_4$	1.125	1.163
6322.6936	207	$b\,^3F_3 - y\,^3F^o_4$	1.500	1.505
6335.3378	62	$a\,^5P_2 - y\,^5D^o_3$	1.167	1.164
6336.8328	816	$z\,^5P^o_1 - e\,^5D_1$	2.000	2.002
6380.7483	1015	$c\,^3F_2 - w\,^3F^o_2$	0.667	0.677
6392.5429	109	$a\,^3P_2 - y\,^5D^o_1$	1.500	1.513
6393.6113	168	$a\,^3H_5 - z\,^5G^o_4$	0.800	0.908
6408.0262	816	$z\,^5P^o_1 - e\,^5D_2$	1.000	1.011
6411.6586	816	$z\,^5P^o_2 - e\,^5D_3$	1.167	1.181
6419.9559	1258	$y\,^3D^o_3 - f\,^3D_3$	1.333	1.291
6430.8538	62	$a\,^5P_3 - y\,^5D^o_4$	1.250	1.241
6436.4102	1016	$c\,^3F_2 - v\,^3D^o_1$	0.750	0.734
6475.6318	206	$b\,^3F_4 - z\,^3G^o_3$	2.000	1.901
6481.8784	109	$a\,^3P_2 - y\,^5D^o_2$	1.500	1.500
6494.9910	168	$a\,^3H_6 - z\,^5G^o_5$	0.917	1.025
6498.9461	13	$a\,^5F_3 - z\,^7F^o_3$	1.375	1.381
6518.3736	342	$b\,^3P_2 - y\,^3D^o_3$	1.167	1.150
6574.2325	13	$a\,^5F_2 - z\,^7F^o_2$	1.250	1.252
6575.0229	206	$b\,^3F_3 - z\,^3G^o_3$	0.917	0.932
6581.2143	34	$a\,^3F_4 - z\,^5F^o_4$	1.300	1.304
6593.8798	168	$a\,^3H_5 - z\,^5G^o_5$	1.150	1.128
6608.0301	109	$a\,^3P_2 - y\,^5D^o_3$	1.500	1.478
6609.1189	206	$b\,^3F_4 - z\,^3G^o_4$	1.150	1.167
6625.0272	13	$a\,^5F_1 - z\,^7F^o_1$	0.750	0.767
6633.7562	1197	$y\,^5P^o_3 - e\,^5P_3$	1.667	1.662
6646.9355	206	$b\,^3F_2 - z\,^3G^o_3$	0.833	0.919
6653.9110	1052	$y\,^3D^o_3 - e\,^3F_3$	1.292	1.215
6663.4503	111	$a\,^3P_1 - z\,^3P^o_0$	1.500	1.500
6677.9958	268	$a\,^3G_5 - y\,^3F^o_4$	1.100	1.099
6703.5720	268	$a\,^3G_3 - y\,^3F^o_3$	0.917	0.921
6704.4794	1052	$y\,^5D^o_1 - e\,^3F_2$	0.250	0.187
6710.3213	34	$a\,^3F_4 - z\,^5F^o_5$	1.700	1.689
6712.4670	1279	$x\,^5D^o_2 - f\,^3F_3$	0.667	0.641
6725.3640	1052	$y\,^5D^o_4 - e\,^3F_4$	1.375	1.392
6726.6722	1197	$y\,^5P^o_2 - e\,^5P_1$	1.500	1.538
6733.1567	1195	$y\,^5P^o_1 - g\,^5D_0$	2.500	2.502
6739.5243	34	$a\,^3F_3 - z\,^5F^o_3$	1.167	1.168
6745.9626	1005	$c\,^3F_4 - w\,^5G^o_3$	1.750	1.763
6746.9508	205	$b\,^3F_2 - z\,^5G^o_2$	0.500	0.499
6750.1597	111	$a\,^3P_1 - z\,^3P^o_1$	1.500	1.498
6786.8632	1052	$y\,^5D^o_2 - e\,^3F_3$	0.667	0.719
6793.2656	1005	$c\,^3F_4 - w\,^5G^o_4$	1.200	1.204
6806.8491	268	$a\,^3G_4 - y\,^3F^o_4$	1.150	1.148
6810.2669	1197	$y\,^5P^o_2 - e\,^5P_3$	1.500	1.492
6828.5976	1195	$y\,^5P^o_1 - g\,^5D_2$	1.000	1.10?
6839.8340	205	$b\,^3F_4 - z\,^5G^o_4$	1.200	1.169
6841.3450	1195	$y\,^5P^o_2 - g\,^5D_3$	1.167	1.148
6842.6903	1197	$y\,^5P^o_1 - e\,^5P_1$	2.500	2.467
6843.6606	1173	$y\,^3F^o_4 - e\,^3D_3$	1.125	1.097
6855.1684	1195	$y\,^5P^o_3 - g\,^5D_4$	1.250	1.226
6857.2481	1006	$c\,^3F_4 - z\,^1G^o_4$	1.125	1.144
6858.1540	1173	$y\,^3F^o_3 - e\,^3D_2$	1.000	1.047

those determined statistically (from the Sun) lie close together. The exceptions are 4798.3 Å ($g_{LS}=0.833$, $g_{lab}=1.167$, $g_{sun}=1.4$) and 5236.2 Å ($g_{LS}=0.250$, $g_{lab}=0.39$, $g_{sun}=0.6$). When deriving the g_{eff} values from the solar data we of course compensated for their χ_e dependence using (7) below. The wavelength dependence is insignificant and can be neglected.

For almost a quarter of the lines selected by Stenflo and Lindegren (1977) no empirical g values were found for at least one of the levels. All but two of the lines for which empirical g_{eff} values were determined in Table 1 of Paper I fall into this category, so that we cannot compare their g_{eff} values as derived by the two different methods. They have accordingly not been included in our Table 2. For the two lines (4596.4 and 4945.6 Å) for which a comparison is possible, this has already been carried out in Paper I.

3. Statistical analysis and interpretation of the scatter plots

3.1. Line profile parameters and their scatter plots

The parameterization of the line profiles is exactly the same as in Paper I, so we will only list the parameters which are of consequence for the present work. Parameters of the I profile are marked by an index I, those of the I_V profile by an index V. The parameters are: (a) Line depth d_I and d_V. (b) Line strength S_I and S_V, defined as the profile area in Fraunhofer below the half level chord of the profile. (c) Line width v_{D_I} and v_{D_V}, in velocity units (km s^{-1}), defined as the Doppler width of a Gaussian profile that has the same half-level width (at the level halfways between the continuum and the line bottom) as the observed profile. (d) Area asymmetry of Stokes V, $\Delta A = A_b - A_r$. (e) Amplitude asymmetry of Stokes V, $\Delta a = a_b - a_r$.

When the line parameters have been determined, we can start looking for effects introduced by adding the Fe II lines to some of the scatter plots discussed in Paper I.

Let us first look at the dependence of $v_{D_V} - v_{D_I}$ on S_I for Fe I and Fe II lines shown in Fig. 2. The stars denote Fe I lines with $\chi_e < 3$ eV, the circles Fe I lines with $\chi_e \geqq 3$ eV, and the filled squares Fe II lines. In subsequent plots these symbols will be retained unless otherwise mentioned. The number of Fe II lines is small, in particular the number of strong ones, which makes the statistics less well established as compared with the Fe I lines. Nevertheless there appears to be a trend for the stronger Fe II lines to lie above their Fe I counterparts. By replacing the excitation potentials, χ_e, by $\chi^* = \chi_i + \chi_e$, where $\chi_i = 0.0$ eV for Fe I and 7.87 eV for Fe II (representing the ionization potential of neutral iron), we can see that the positions of the Fe II lines in the $v_{D_V} - v_{D_I}$ vs. S_I diagram cannot be extrapolated from the positions of Fe I lines with different χ^*.

The indication that Fe II lines retain their widths in fluxtubes, in contrast to the Fe I lines, seems natural in view of their reduced temperature sensitivity. However, this expectation is inconsistent with the trend for highly excited Fe I lines to lie below less highly excited ones in the scatter plot of Fig. 2. This behaviour is also reflected in the amplitude asymmetries of the two ionization species, plotted as a function of S_I in Fig. 3. The areas with light shading indicate the location of Fe I points with $\chi_e \geqq 3$, the areas with intermediate shading Fe I with $\chi_e < 3$, and the areas with dark shading Fe II lines. Again the behaviour of the Fe II lines does not follow from an extrapolation of the Fe I lines. They are too asymmetric as compared with the highly excited Fe I lines. This is however entirely consistent with the behaviour in Fig. 2 if we

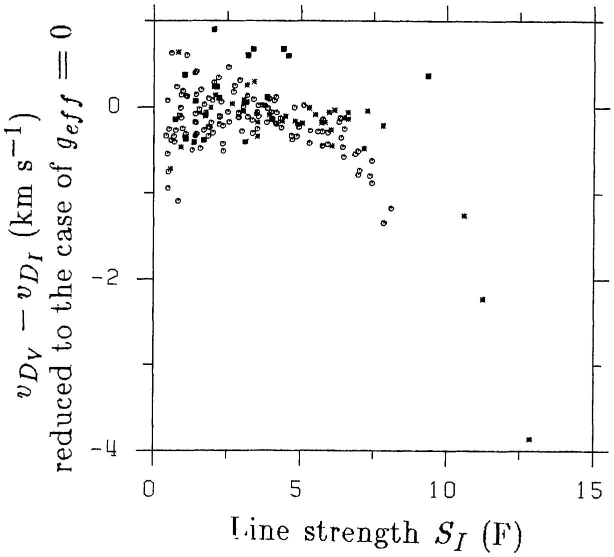

Fig. 2. Difference in line width of the I_V and I profiles, $v_{D_V} - v_{D_I}$, plotted vs. I line strength, S_I, for an enhanced network region. The line widths have been reduced to the case that $g_{eff}=0$. Fe I lines with $\chi_e<3$ eV are represented by stars, those with $\chi_e \geqq 3$ eV by circles, and the Fe II lines by filled squares

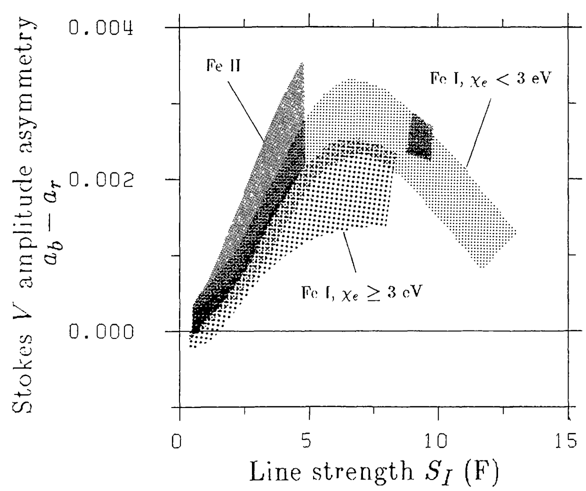

Fig. 3. Absolute amplitude asymmetry $\Delta a = a_b - a_r$ vs. S_I for an enhanced network region. a_b and a_r are the amplitudes of the blue and red wings of Stokes V in units of the intensity of the adjacent continuous spectrum. The lightly shaded portions indicate the location of Fe I lines with $\chi_e \geqq 3$ eV, the intermediately shaded portions Fe I lines with $\chi_e<3$ eV, and the darkly shaded portions Fe II lines. The absolute values of the asymmetry in Fig. 5 of Paper I are larger than the values plotted here because the former showed data from a plage. The values of the relative asymmetries are comparable for both regions

assume as in Paper I that the velocity gradient required to explain the presence of V asymmetries (Auer and Heasley, 1978) induces an increase in line width proportional to the amplitude asymmetry.

Our attention in the present paper will mainly concern the plots of $\ln(d_V/d_I)$ vs. S_I and $\ln(d_V/d_I)$ vs. χ_e. Figure 4 shows $\ln(d_V/d_I)$ of Fe I and Fe II lines recorded in a network region plotted vs. S_I. Here the Fe II lines behave as expected and lie, at least for small values of S_I, well above the Fe I lines. For strong lines $\ln(d_V/d_I)$ seems to be practically independent of χ^*, although the statistics is rather poor.

We can extend the regression analysis of $\ln(d_V/d_I)$ presented in Sect. 3.2 of Paper I to include the Fe II lines if we replace χ_e by χ^*.

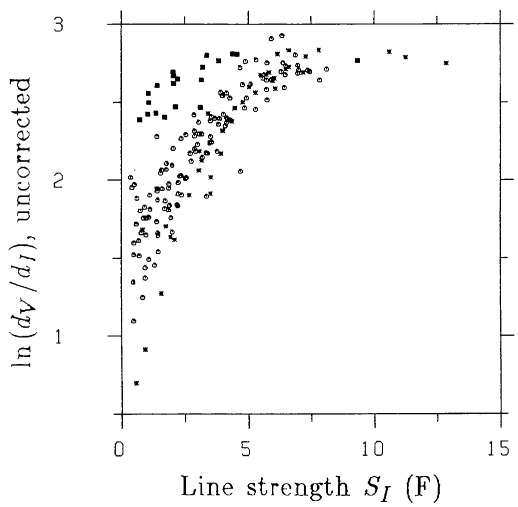

Fig. 4. The logarithm of the ratio of the line depths of I_V and I, $\ln(d_V/d_I)$, plotted vs. S_I for an enhanced network region. The symbols are the same as in Fig. 2

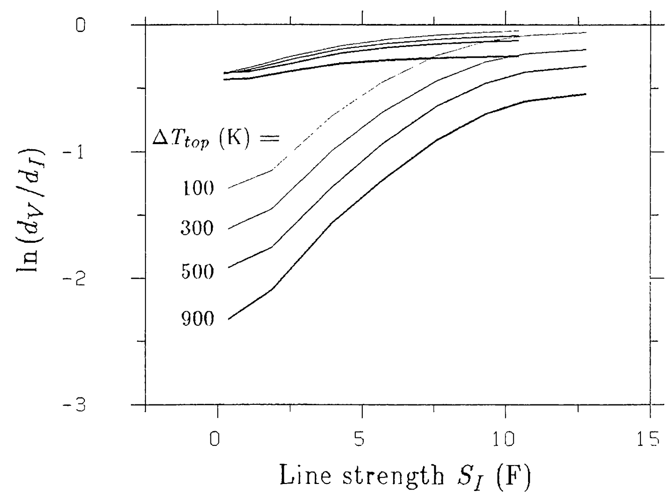

Fig. 5. $\ln(d_V/d_I)$ vs. S_I for four models with $f=\xi_{t_{\rm fluxtube}}/\xi_{t_{\rm photosphere}}=0.7$, Wilson depression $Z_W=60$ km, $\Delta T_{\rm bot}=750$ K, and $\Delta T_{\rm top}=100, 300, 500$, and 900 K in the order of increasing thickness of the curves. The almost horizontal curves correspond to Fe II lines, the others to Fe I lines. All the curves are unshifted

However, the use of the regression equation for $\ln(d_V/d_I)$ presented in Paper I,

$$\ln(d_V/d_I)=x_1+x_2S_I+x_3S_I^2+x_4\chi^* +x_5S_I\chi^*+x_6g_{\rm eff}^2\lambda^2/v_0^2\,, \tag{6}$$

does not lead to a proper description of the χ^* dependence of $\ln(d_V/d_I)$ of Fe I and Fe II simultaneously. A considerable improvement is achieved if

$$\ln(d_V/d_I)=x_1+x_2S_I+x_3S_I^2+x_4\chi^* +x_5\chi^*h(S_I)+x_6g_{\rm eff}^2\lambda^2/v_0^2 \tag{7}$$

is used instead, where $h(S_I)=S_I+a_1S_I^2+a_2S_I^3$. Thus two new regression coefficients, a_1 and a_2, need to be determined simultaneously with the x_i coefficients. (7) works well for Fe I alone too, and its use instead of (6) does not affect the results of Paper I significantly. In order to reduce the dependence of the results on the exact form of the regression equation we have tried to avoid basing them on a regression analysis whenever possible. This may be unnecessarily cautious, since the results obtained by comparing model calculations with data before and after applying (7) do not differ greatly.

The lack of sensitivity of the Fe II lines to temperature causes their $\ln(d_V/d_I)$ values to be practically independent of line strength. It should also make the absolute values of $\ln(d_V/d_I)$ lie close to zero (since the line weakening is small). The precise value of the line weakening can however only be determined by comparison with model calculations.

The scatter plots having $g_{\rm eff}^2\lambda^2/v_0$ or $g_{\rm eff}^2\lambda^2/v_0^2$ as abscissa remain largely unaffected by the addition of the Fe II lines. In particular the values of the line of sight component of the magnetic field strength are unchanged.

3.2. *Fluxtube models and radiative transfer*

The fluxtube models and radiative transfer routines used are the same as in Paper I, where they have been described in detail. The model is one-dimensional, assumes the HSRA (Gingerich et al., 1971) to be a description of the fluxtube surroundings, and is characterized by four parameters: Z_W, the Wilson depression, $\Delta T_{\rm top}=T_{\rm fluxtube}-T_{\rm HSRA}$ at the geometrical height where $\tau_{5000}({\rm HSRA})=10^{-4}$, $\Delta T_{\rm bot}=\Delta T$ at the level $\tau_{5000}({\rm HSRA})=1$, and $f=\xi_{t_{\rm fluxtube}}/\xi_{t_{\rm HSRA}}$, the ratio of the microturbulence velocities inside and outside the fluxtube. The temperature as a function of height is found by linear interpolation between $\Delta T_{\rm top}$ and $\Delta T_{\rm bot}$ [the resulting $\Delta T(\tau)$ is approximately linear]. We must stress again that this very crude model only serves as an exploratory tool to gain insight into the diagnostic contents of the scatter plots.

The radiative transfer calculations have been carried out using an LTE code capable of calculating all four Stokes parameters for a general model atmosphere and magnetic field structure (Beckers, 1969a, b). The calculated Fe I lines are represented by the 96 hypothetical lines mentioned in Paper I. Eight hypothetical Fe II lines, all having a wavelength of 5000 Å, an excitation potential of 3 eV, and a Landé factor of unity, but with varying oscillator strengths, were calculated for each. This choice of χ_e and $g_{\rm eff}$ corresponds to the typical values of these quantities in the Fe II line list used. We refrained from studying the effects of varying Landé factor and excitation potential due to the small ranges of variation of these quantities for the observed lines, and also due to the small number of lines. As a matter of fact we did calculate the profiles of Fe II lines with $\chi_e=2.5$ and $\chi_e=4.0$ eV. The resulting effects in the profiles due to the change in χ_e were very small, much smaller than the scatter in the data, and would hardly have been visible in Figs. 5, 6, or 7. The same is true for the wavelength and Landé factor dependences of the line profiles. Thus by choosing a wavelength of 5000 Å, a $g_{\rm eff}$ of 1.0, and a χ_e value of 3 eV we are making a very good approximation for almost all the lines.

3.3. *Insights from the comparison of theory and observations*

Let us take a closer look at the $\ln(d_V/d_I)$ vs. S_I plot. The curves calculated from four different models are plotted in Fig. 5. Each model is represented by two curves, one for Fe I lines with $\chi_e=0$, the lines running from upper right to lower left, and one for Fe II lines with $\chi_e=3$, the almost horizontal lines at the top of the plot.

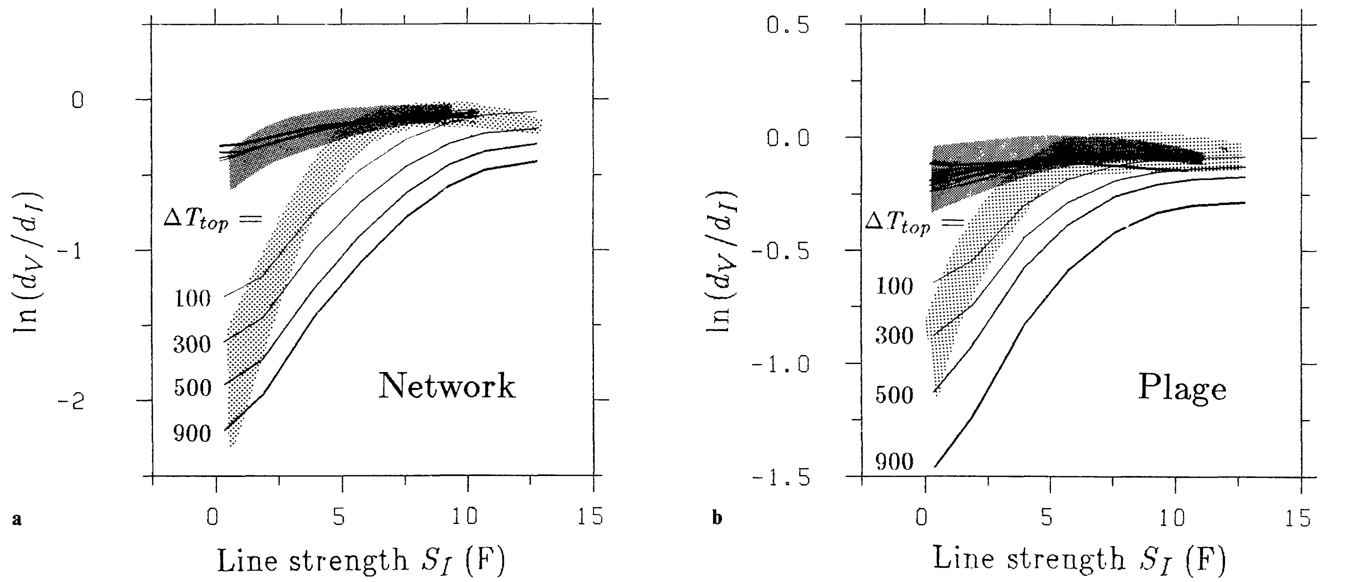

Fig. 6a and b. Comparison of model calculations with observations: $\ln(d_V/d_I)$ vs. S_I. **a** Enhanced network data (Light shading: Fe I lines with $\chi_e=0$; dark shading: Fe II lines with $\chi_e=3$ eV) plotted together with the model curves of Fig. 5. The empirical data and the model curves have been shifted such that the results for Fe II overlap. **b** Plage data (Light shading: Fe I lines with $\chi_e=0$; dark shading: Fe II lines with $\chi_e=3$ eV) plotted together with model curves using $f=0.7$, $Z_W=60$ km, $\Delta T_{\rm bot}=250$ km, and $\Delta T_{\rm top}=100$, 300, 500, and 900 K (in the order of increasing thickness of the curves). All curves have been shifted such that the results for Fe II overlap

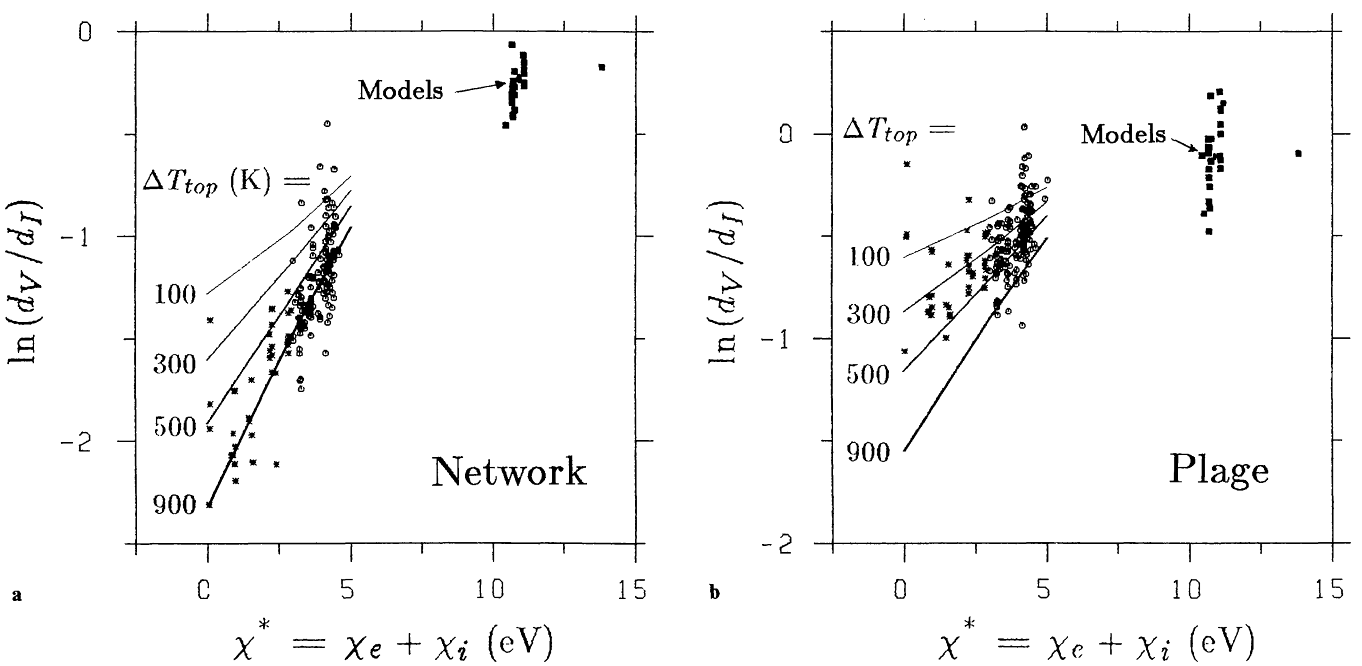

Fig. 7a and b. Comparison of model calculations with observations: $\ln(d_V/d_I)$ vs. χ^*. **a** Enhanced network data reduced to the case that $S_I=0$ and $g_{\rm eff}=0$ using (7), plotted together with the curves for very weak lines calculated using the four models of Fig. 5. The data have been shifted such that the models provide good fits to the Fe II lines. **b** Plage data reduced to the case of $S_I=0$ and $g_{\rm eff}=0$ using (7), plotted together with the curves for very weak lines calculated using the four models of Fig. 6b. The data have been shifted such that the models provide good fits to the Fe II lines. Since the values of $\ln(d_V/d_I)$ for Fe II derived from the various models almost coincide, their locations are collectively indicated by a single arrow

The chosen models all have $Z_W=60$ km and $f=0.7$. The choice of these parameters is not critical, since this diagram is practically independent of both of them. All the models also have $\Delta T_{\rm bot}=750$ K, which was found to give a reasonably good fit to the shape of the $\ln(d_V/d_I)$ vs. S_I network data for the Fe I lines in Paper I. The only variable parameter is $\Delta T_{\rm top}$, which has been given values of 100, 300, 500, and 900 K for the four models shown.

We notice that the change in the temperature at $\tau_{5000}=10^{-4}$ affects the shape of the curves only slightly in our linear $\Delta T(\tau)$ models. The main effect is to shift the curves vertically. Thus an increase of $\Delta T_{\rm top}$ results in a decrease of $\ln(d_V/d_I)$. The Fe I curves are shifted by a much larger amount than the Fe II curves. This behaviour is no surprise, since the line weakenings are expected to increase with fluxtube temperature, and the dependence of line weakening on temperature should be stronger for Fe I lines. With the additional use of the Fe II lines we can therefore obtain a relatively model independent value of the line weakening, i.e., we can determine an absolute scale for the line depths and strengths of the I_V profiles. At the same time we obtain a value of $\Delta T_{\rm top}$.

Figure 6a illustrates how such a determination can be carried out. Here, the empirical data from a network region are plotted together with the model curves of Fig. 5. The lightly shaded portion represents Fe I lines with $\chi_e=0$ (the lower envelope of the Fe I lines in Fig. 4), the darkly shaded portion Fe II lines with $\chi_e=3$ (average of the Fe II lines in Fig. 4). These empirical data have not been modified by any regression analysis. The zero point for the empirical data has been shifted, so that the observed Fe II lines match the calculated Fe II curve for the model with $\Delta T_{\rm top}=300$ K. It should be noted that the vertical shift used for the empirical data is the same for both Fe I and Fe II, so that their *relative* positions remain unchanged. The curves calculated from the other three models have also been shifted slightly to fit the Fe II data (again the Fe I and Fe II curves have been shifted by the same amount). The correct $\Delta T_{\rm top}$ is obtained from the model that fits the Fe I and Fe II data simultaneously. Our simple models suggest that the temperature of the network fluxtubes at the top of the photosphere does not exceed the temperature of the surroundings by more than 300 K.

The same method is applied to a plage region in Fig. 6b. The models plotted here differ from those in Fig. 6a by having $\Delta T_{\rm bot}=250$ K, found to be the best fit plage temperature at $\tau_{5000}=1$ in Paper I. Now the model curves lie closer together, but $\Delta T_{\rm top}$ still seems to be less than 500 K.

How do these results compare with the evidence presented by other plots? They are consistent with the $v_{D_V}-v_{D_I}$ vs. S_I plot, although it is difficult to differentiate between the models in this plot. More interesting is the $\ln(d_V/d_I)$ vs. χ^* plot shown in Fig. 7a for a network element, the observed data being reduced to the case that $S_I=0$ and $g_{\rm eff}=0$ by using (7). Superimposed are curves derived from the models already used for Fig. 6a. This time it is the models with higher $\Delta T_{\rm top}$ which provide the better fit. This apparent contradiction with the results of the $\ln(d_V/d_I)$ vs. S_I plot probably arises from the fact that the $\ln(d_V/d_I)$ vs. χ^* plot has been reduced to $S_I=0$ and is mainly sensitive to temperature changes lower down in the fluxtube. Changes in $\Delta T_{\rm top}$ affect this diagram through the induced change at the lower levels due to the linear height interpolation of ΔT. Thus by demanding that a model should simultaneously fit the data in both plots we can determine the height dependence of ΔT. Figure 7b shows $\ln(d_V/d_I)$ vs. χ^* for data from a plage region and the four plage models already used in Fig. 6b. Here the consistency between the $\ln(d_V/d_I)$ vs. S_I and $\ln(d_V/d_I)$ vs. χ^* plots is better, suggesting that $\Delta T(\tau)$ does not deviate so strongly from a linear function as in network fluxtubes.

3.4. *Influence of magnetic filling factor and fluxtube expansion on the derived temperatures*

The magnetic filling factor, α, represents the fraction of the surface area covered by the fluxtubes at $\tau_{5000}=1$. For expanding fluxtubes this fraction will increase with height. Let us now consider the effects that α and the fluxtube expansion can have on the fluxtube temperature structure as derived from the $\ln(d_V/d_I)$ vs. S_I plot. The effect comes mainly via the observed I profiles, which are "contaminated" by light from the fluxtubes. Ideally (for small α), the I profiles represent the non-magnetic surroundings of the fluxtubes. However, the larger the α, the larger the I_V component of I will be, which causes an apparent decrease of the temperature difference between the fluxtubes and their surroundings. For fluxtubes whose diameters are independent of height this contamination will result in a shallower $\ln(d_V/d_I)$ vs. S_I plot. Fluxtube expansion will tend to lessen this effect and if it is strong enough may actually result in a steeper $\ln(d_V/d_I)$ vs. S_I plot.

Although these effects cannot be reproduced by our simple fluxtube model, so that in its present form it cannot give us any information on the shape of the fluxtube, there is fortunately a method of checking the validity of the derived temperatures without having to resort to the use of a two dimensional model. This was attempted in Paper I by replacing the plage I profiles by their network counterparts and determining $\Delta T_{\rm bot}$ from $\ln(d_V(\text{plage})/d_I(\text{network}))$ vs. S_I. In the present work we have gone a step further and have used recordings of Stokes I in a quiet region made at disk center with the McMath FTS on April 29, 1979. Using the quiet-region Stokes I instead of I profiles in active regions does not change the relative positions of the Fe I and Fe II lines in the $\ln(d_V/d_I)$ vs. S_I plots. Although the gradients of the $\ln(d_V/d_I)$ vs. S_I curves of plages are increased, so that they lie closer to the network curves, a distinct difference between plages and network still remains. It thus seems that the effects of filling factor and fluxtube expansion do not invalidate the results of the one-dimensional models. More subtle radiative transfer effects coupled with the fluxtube geometry could however still play a significant role.

4. Results and discussion

We have extended the analysis presented in Paper I to lines of singly ionized iron to allow the determination of an additional fluxtube parameter, $\Delta T_{\rm top}$. With our crude model, used mainly as an exploratory tool, we find the values of $\Delta T_{\rm top}$ to be below 500 K. For the network regions the results are also compatible with no temperature excess at all in the uppermost portion of the photospheric fluxtube. This is comparable to the temperature found by Cook et al. (1983), but is not consistent with results of other models, for example Stenflo (1975), Chapman (1979), Koutchmy and Stellmacher (1978), and Stellmacher and Wiehr (1979).

One possible reason for this difference may be that the regions of highest temperature need not always be cospatial with those having the greatest magnetic field strength (Simon and Zirker, 1974; Koutchmy and Stellmacher, 1978). Since our results for $\Delta T_{\rm top}$ are largely based on the behaviour of the strong lines, non-LTE effects may also be important. Finally, the selection of a nonlinear τ-variation of ΔT should affect the derived $\Delta T_{\rm top}$ and $\Delta T_{\rm bot}$ values considerably. The study of the effects of different temperature stratifications will be the subject of a future investigation.

After the effects of the magnetic filling factors have been taken into account, $\Delta T_{\rm bot}=350$–600 K for plages, and 800–1200 K for the network. Thus a considerable difference in fluxtube temperature structure between the plages and network still remains.

The magnetic filling factors of the observed regions can be determined simply from the amount by which the empirical curves in the $\ln(d_V/d_I)$ vs. S_I plot have to be shifted to fit the model curves, and from the magnetic field strengths (given in Table 2 of Paper I for the five regions studied). The additional use of Fe II makes this procedure relatively model independent, since all the model curves lie closely together. The uncertainty in the α values resulting from their model dependence is no more than a few percent, and is comparable to the uncertainty caused by the scatter of the Fe II points. If we multiply the derived α values with a factor of two to account for an instrumental calibration error in accordance with Stenflo and Harvey (1985), we find values for the magnetic filling factor between 1.5 and 14.5%. The network filling factors are approximately half as large as those given in Table 2 of Paper I, whereas the plage filling factors are almost unaffected.

The present exploratory investigation has brought out the diagnostic contents of the Fe I and II lines for fluxtube modelling, and has indicated some of the gross features of the fluxtube temperature structure. For a more definite empirical determination of the fluxtube structure we need models with a more general temperature-density structure. Ideally these would be self-consistent two-dimensional MHD fluxtube models with diverging geometry.

Acknowledgements. We would like to thank Dr. U. Litzén for his help in the compilation of the empirical Landé factors.

References

Auer, L.H., Heasley, J.N.: 1978, *Astron. Astrophys.* **64**, 67

Beckers, J.M.: 1969a, *Solar Phys.* **9**, 372

Beckers, J.M.: 1969b, *Solar Phys.* **10**, 262

Beckers, J.M.: 1969c, A Table of Zeeman Multiplets, AFCRL-69-0115

Chapman, G.A.: 1979, *Astrophys. J.* **232**, 923

Cook, J.W., Brueckner, G.E., Bartoe, J.-D.F.: 1983, *Astrophys. J.* **270**, L 89

Corliss, C., Sugar, J.: 1982, *J. Phys. Chem. Ref. Data* **11**, No 1, 353

Dravins, D., Larsson, B.: 1984, in *Small-Scale Dynamical Processes in Quiet Stellar Atmospheres*, ed. S.L. Keil, National Solar Observatory (in press)

Gingerich, O., Noyes, R.W., Kalkofen, W., Cuny, Y.: 1971, *Solar Phys.* **18**, 347

Koutchmy, S., Stellmacher, G.: 1978, *Astron. Astrophys.* **67**, 93

Landi Degl'Innocenti, E.: 1982, *Solar Phys.* **77**, 285

Litzén, U.: 1984 (private communication)

Moore, C.E.: 1952, Atomic Energy Levels, National Bureau of Standards

Reader, J., Sugar, J.: 1975, *J. Phys. Chem. Ref. Data* **4**, 353

Simon, G.W., Zirker, J.B.: 1974, *Solar Phys.* **35**, 331

Solanki, S.K., Stenflo, J.O.: 1984, *Astron. Astrophys.* **140**, 185

Stellmacher, G., Wiehr, E.: 1979, *Astron. Astrophys.* **75**, 263

Stenflo, J.O.: 1975, *Solar Phys.* **42**, 79

Stenflo, J.O., Lindegren, L.: 1977, *Astron. Astrophys.* **59**, 367

Stenflo, J.O., Harvey, J.W., Brault, J.W., Solanki, S.K.: 1984, *Astron. Astrophys.* **131**, 333

Stenflo, J.O., Harvey, J.W.: 1985, *Solar Phys.* **95**, 99